Optics Letters

Broadband mid-infrared coverage (2–17 μm) with few-cycle pulses via cascaded parametric processes

Qing Wang,[1,2,†,*] Jinwei Zhang,[1,†] Alexander Kessel,[1] Nathalie Nagl,[3] Vladimir Pervak,[3] Oleg Pronin,[1] and Ka Fai Mak[1]

[1]Max-Planck Institute of Quantum Optics, Hans-Kopfermann-Str. 1, 85748 Garching, Germany
[2]School of Optics and Photonics, Beijing Institute of Technology, 5 South Zhongguancun Street, 100081 Beijing, China
[3]Ludwig-Maximilians Universität München, Am Coulombwall 1, 85748 Garching, Germany
*Corresponding author: qingwang@bit.edu.cn

Received 15 February 2019; revised 24 March 2019; accepted 10 April 2019; posted 12 April 2019 (Doc. ID 360259); published 15 May 2019

A myriad of existing and emerging applications could benefit from coherent and broadband mid-infrared (MIR) light. Yet, existing tabletop sources are often complex or sensitive to interferometric optical misalignment. Here we demonstrate a significantly simplified scheme of broadband MIR generation by cascading the intra-pulse difference-frequency generation process in a specific nonlinear crystal. This allows pulses generated directly from mode-locked lasers to be used without further nonlinear temporal compression. The system, together with the driving beam, can provide an ultra-broadband coherent radiation coverage ranging from 2 to 17 μm with femtosecond pulse durations. To the best of our knowledge, this is the first demonstration of cascaded DFG in the MIR range, which brings emerging time-domain spectroscopic techniques closer to real-world applications.

https://doi.org/10.1364/OL.44.002566

Radiation in the mid-infrared (MIR) [2–20 μm] supports a plethora of applications and is particularly useful in chemical and biological identification due to the presence of many characteristic absorption lines ("fingerprints") in this spectral region [1,2]. These features have been extensively utilized in the past by pairing incoherent thermal MIR sources with Fourier-transform infrared spectroscopy [3]. However, the use of spatially coherent sources, especially those in the form of frequency combs or femtosecond pulses, creates a completely new range of possibilities such as micro-spectroscopy [4,5], sensitive measurements with high dynamic range [6,7], and femtosecond pump-probe spectroscopy [8]. Currently available coherent MIR sources such as synchrotron beam lines [9], quantum cascade lasers [10], supercontinuum sources [5,11], and optical parametric oscillators and amplifiers [4,12–14] have their own advantages and disadvantages in terms of accessibility, spectral bandwidth, pulse duration, output power, and stability.

Intra-pulse difference-frequency generation (IDFG) is a parametric technique that removes the need to overlap two separate beams at interferometric precision [15,16], while providing few-cycle pulses with intrinsic carrier-envelope phase (CEP) stabilization. The technique is becoming popular for MIR generation, thanks to the recent emergence of high-power femtosecond 2 μm lasers that can effectively pump small-bandgap non-oxide crystals transparent in the MIR. The first demonstration of broadband IDFG pumped at 2 μm was undertaken using a thin-disk laser [17] and soon after demonstrated using other systems [18,19].

However, the shortest MIR wavelength that can be generated via simple IDFG is dictated by the difference between the lowest and highest frequency components of the input pulse. To generate MIR light at a wavelength of 4.5 μm or a frequency of 67 THz, for example, a pump pulse with spectral components separated by the same frequency span is required, which is equivalent to a ∼11 fs pulse at a central wavelength of 2.3 μm (full-width at $1/e^2$ of maximum). To generate such pump pulses at 2 μm, dedicated nonlinear pulse compression stages are usually employed [17,18], which significantly increase the complexity and reduce the reliability of the setup.

In contrast to previous approaches, we demonstrate that, by cascading the parametric mixing in a suitable semiconductor crystal, few-cycle pulses with a multi-octave-spanning MIR continuum can be generated using driving pulses that are up to eight times longer than those required by conventional IDFG alone. Consequently, a mode-locked Cr:ZnS solid-state oscillator, followed by an amplification stage, already provides sufficiently short driving pulses, eliminating the need for dedicated nonlinear pulse compression stages. This use of a Cr:ZnS laser as a driving source for IDFG was first reported in Ref. [20] and, recently, by Vasilyev *et al.* [21]. The robust single-beam geometry of IDFG can already provide ultra-broadband output that is likely to be few-cycle in pulse duration and passively CEP-stabilized. By further exploiting the cascading parametric effect and employing compact and mature laser systems as direct pump sources, the presented scheme is among the most attractive techniques for generating coherent broadband MIR.

As mentioned earlier, new spectral components at lower frequencies are generated when the components of an initial driving pulse are nonlinearly mixed together. However, the generated spectrum can be further mixed with the initial pump to generate even more frequency components—a process recently observed in the near infrared to generate a broadband continuum [22,23]. An example of such processes in the MIR, simulated using a one-dimensional (1D)+time split-step method [22], is shown in Fig. 1(a). For clearer insights, the high and low frequency components of a single driving pulse are represented by two separate beams at 2.1 and 2.5 μm. These two beams first interact in a GaSe crystal to generate the fundamental DFG signal centered at 13 μm. Upon further propagation, the 13 μm beam re-mixes with the original 2.5 μm beam to generate additional DFG signals at 3.1 μm, which further mixes with the original 2.1 μm to generate radiation at 6.6 μm. As shown in Fig. 1(b), thanks to the unique phase-matching (PM) characteristics of GaSe, all of these processes occur at a very similar PM angle. For example, the first cascaded process can be seen as the 2.5 μm pump interacting with the 13 μm component, which functions as the idler. As shown, the generated signal at 3.1 μm is also phase-matched at ∼11°. Apart from the cascaded DFG processes, sum-frequency generation processes also occur between the different components, generating new signals below 2.1 μm [red components in Fig. 1(a)]. When an initial broadband pulse (instead of the two distinct beams) is used, the correspondingly broader cascading peaks will overlap with each other, forming an ultra-broad continuum. In the following section, we describe the experimental implementation of such a scheme, using ∼30 fs pulses from a home-built Cr:ZnS master-oscillator power-amplifier laser system.

The schematic of the experimental setup is shown in Fig. 2. Both the oscillator and the amplifier use polycrystalline Cr:ZnS as the gain medium, which is at a normal-incidence angle to reduce asymmetric thermal lensing effects, similar to Refs. [24,25]. The Kerr-lens mode-locked oscillator directly emits pulses with durations of 45 fs, at an average power of over 1 W. This is equivalent to ∼15 nJ of pulse energy at a

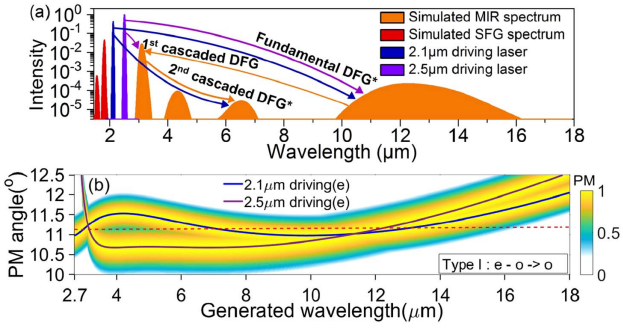

Fig. 1. (a) Simulated output spectra arising from cascaded nonlinear processes driven by two narrow-band pulses. The different frequency-mixing products are labeled with their order of appearance during propagation and the underlying frequency-mixing processes. Spectral components marked with an asterisk are, in principle, are passively CEP stable. (b) Optimal PM angle and PM function PM = $|\mathrm{sinc}(\Delta kL/2)|$ in GaSe with respect to the generated signal (idler wavelengths) with either a 2.1 (blue curve) or 2.5 μm (purple curve) beam acting as the pump beam. The red dashed line indicates the approximate PM angle used in the experiment.

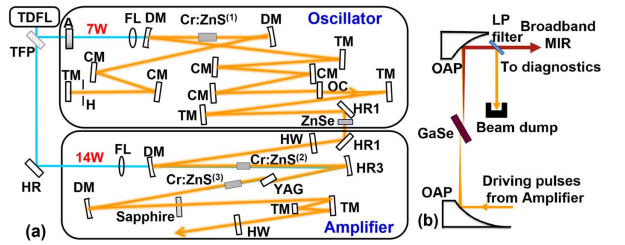

Fig. 2. (a) Kerr-lens mode-locked Cr:ZnS oscillator and amplifiers. TDFL, Tm-doped fiber laser (1908 nm). A, attenuator; FL, focusing lens ($f = 75$ mm); DM, curved dichroic mirror (ROC = −100 mm); CM, chirped mirror (GDD ≈ −200 fs^2 per bounce); TM, third-order dispersion mirror (TOD ≈ −3200 fs^3 per bounce); OC, output coupler (OC, 32%); HR3, curved high reflection (HR at 1.9–3.0 μm, ROC = −100 mm); H, hard aperture; HW, half-wave plate; Cr:ZnS$^{(1)}$, Cr:ZnS$^{(3)}$, ($5 \times 2 \times 9$ mm^3, $T = 15\%$ at 1908 nm); Cr:ZnS$^{(2)}$, ($5 \times 2 \times 6$ mm^3, $T = 20\%$ at 1908 nm). (b) Schematic of the MIR generation setup. LP, long-pass.

repetition rate of 68.7 MHz. The output is subsequently sent through a two-pass amplifier, which increases the output power to 3.35 W, with a beam quality of $M_x^2 = 1.25$ and $M_y^2 = 1.21$. Due to the high optical nonlinearity of polycrystalline ZnS, the spectrum is slightly broadened during the amplification stage itself [25], resulting in an output pulse duration of 28 fs after phase compensation (3 mm sapphire, three third-order dispersion mirrors, and one half-wave plate), as shown in Fig. 3.

To generate MIR radiation via cascaded IDFG, GaSe crystal was identified as the most suitable nonlinear crystal, due to its large nonlinear coefficient ($d_{\mathrm{eff}} = 54.4$ pm/V), large transmission bandwidth (0.65 to 20 μm) [26], and very broad PM bandwidth when pumped around 2 μm [Fig. 1(b)]. Besides, GaSe has a high optical damage threshold at 2 μm and high thermal conductivity [22]. For these reasons, it has been frequently used for MIR and THz generation, and for detection in electro-optic sampling (EOS) schemes [16,27,28].

The 2.3 μm driving pulses are focused into the 1.2 mm thick uncoated GaSe crystal (Ascut Inc.) using a gold 90° off-axis parabolic (OAP) mirror with an effective focal length (EFL) of 20 mm, resulting in a spot diameter of 46 μm at the focus, measured using a rotating-slit beam profiler (NanoScan 2s, Ophir Optronics Inc.). Since the beam experiences strong Fresnel reflectance of ∼18% on the incidence surface of the uncoated GaSe, only 2.7 W of light enters the crystal. Assuming a Gaussian spatial beam profile, the peak intensity of the focus spot is 120 GW/cm^2. Type-I phase matching

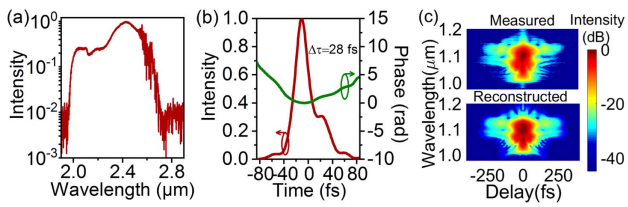

Fig. 3. (a) Measured spectrum of the driving pulse; (b) corresponding temporal profile retrieved from a SHG-FROG measurement, showing a pulse duration of 28 fs; and (c) measured and retrieved SHG-FROG traces of the driving pulse.

is chosen due to its broader PM bandwidth in GaSe, translating to an incident angle of 32° (inner angle is 11.2°). By rotating the GaSe crystal and the half-wave plate behind the amplifier and the GaSe crystal, the incident polarized beam is distributed between the extraordinary and ordinary crystal axes, and the power of the generated MIR radiation is optimized. The MIR beam propagates practically collinearly with the driving beam, and both beams are first collimated by another gold OAP mirror with an EFL of 20 mm before being separated by different long-pass filters (LPFs). The MIR beam is then sent to various diagnostics.

The MIR spectrum is measured using a Czerny—Turner 1/4 m monochromator (Newport Cornerstone 260) with a lithium tantalate pyroelectric detector. The MIR beam is focused into the monochromator using an AR-coated ZnSe lens with a focal length of 100 mm. The monochromator is equipped with a lock-in amplifier and a chopper wheel to improve its sensitivity.

To cover the very broad bandwidth of the generated MIR spectrum, two different monochromator gratings and different LPFs were used to construct the full spectrum, with the relative intensity calibrated using a calibrated silicon nitride infrared source (Bentham Instruments Ltd.). According to the input spectrum [Fig. 3(a)] whose shortest and longest wavelengths are 1.98 and 2.7 μm, the short edge of the generated MIR spectrum should end at 7.5 μm, assuming simple IDFG as the only mixing process. However, the measured MIR spectrum [see Fig. 4(a), blue curve] actually exhibits a peak near 7.5 μm, with a substantial signal detectable at even shorter wavelengths—a strong indication of cascaded DFG. The background level [Fig. 4(a), gray dot curve] is measured by shifting the GaSe 10 mm longitudinally away from the focus, thereby suppressing any nonlinear effects. The background level is also multiplied with the same calibration function, with the peak around 3.0 μm originating from the residual driving beam.

The numerically simulated spectrum [Fig. 4(a), red curve] is calculated using the same 1D+time split-step code mentioned as earlier, but now with the measured spectrum of the driving pulse as input. It matches remarkably well with the experimental results, even though it does not take into account spatial effects such as walk-off, diffraction, and self-focusing. By comparing with the simulation in Fig. 1(a), one can identify that spectral components below 9 μm are attributed to cascaded nonlinear processes. The strong peak at 3 μm is attributed

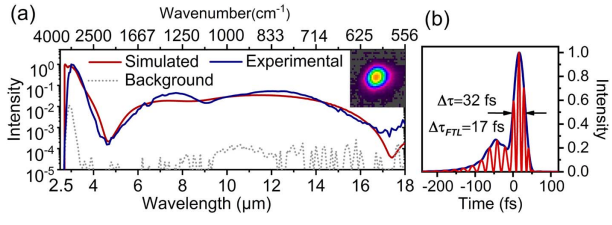

Fig. 4. (a) Experimentally measured spectrum after calibration (blue curve), the corresponding background level (gray dotted curve), and the numerically simulated spectrum (red curve). Inset: beam profile measured using a pyroelectric beam profiler (Pyrocam-III Ophir). (b) Simulated pulse shape (blue curve) and simulated absolute electrical field intensity (red curve) of the MIR above 4.5 μm. The Fourier transform limit calculated from the experimentally measured spectrum (>4.5 μm) is 17 fs.

to the cascaded mixing of the fundamental IDFG signal centered near 12 μm with the pump. Further cascading of the IDFG process results in a broad peak centered at around 7.5 μm, which overlaps with the fundamental IDFG signal. Thanks to the favorable PM condition provided by GaSe [Fig. 1(b)], the magnitude of these components is similar to the fundamental DFG peak, forming a very broad continuum. In contrast to previous IDFG experiments where the components generated via the cascading effect cannot easily be isolated from other nonlinear processes [17–19,21], this is, to the best of our knowledge, the first concrete demonstration of cascaded IDFG in the MIR region. Furthermore, since the continuum at wavelengths longer than 4.5 μm is generated via DFG with an even number of interacting frequency components from the driving beam [see Fig. 1(a)], its CEP should be intrinsically constant [22], which is important for time-domain and frequency-comb applications.

Together with the spectrum of the Cr:ZnS driving laser (1.98 to 2.7 μm) that is co-propagating with the MIR beam [Fig. 3(a)], the system can simultaneously provide coherent radiation spanning over three octaves from 2 to 17 μm. There is a mismatch between the simulation and the experiment at wavelengths beyond 17 μm, which can be attributed to the increased measurement noise and a reduction in reliability for the simulation parameters such as refractive index data at these wavelength ranges. The output power is measured using a thermal power meter (S302C, Thorlabs) to be 15 mW behind a LPF with a cut-on wavelength of 2.8 μm, and 5 mW behind a 4.5 μm cut-on LPF. The output power agrees well with the different integrated area of the measured spectrum. These powers are sufficient to saturate the HgCdTe (MCT) detectors typically used for this wavelength range. Considering the transmission of the LPFs (~70%) and the reflection of the uncoated end surface inside the GaSe (~20%), the actual power is even higher, and the conversion efficiency reaches 0.3% for the >4.5 μm range. The fluctuation in output power, measured over 60 minutes behind the 4.5 μm cut-on LPF is less than 1.3% RMS, even though there have been no major engineering efforts in stabilizing the system, and the beam paths are not sealed against air flow.

Since the simulation agrees well with the experimental MIR spectrum, the temporal characteristics of the MIR pulses were also studied numerically, in particular, for the wavelength region above 4.5 μm that should be intrinsically CEP-stabilized [Fig. 1(a)]. Figure 4(b) shows the simulated temporal profile of the long-wave output (>4.5 μm) along the ordinary axis where 99% of the energy is concentrated. Despite the fact that the pulses contain spectral components originating from both the fundamental and the cascaded IDFG processes, the direct output pulse duration is predicted to remain very short at 32 fs—below two optical cycles for pulses centered at 7 μm. Thus, cascaded IDFG is a promising route for generating femtosecond MIR pulses for ultrafast time-domain applications.

The numerical code is also employed to investigate the pumping with even longer pulse durations such as 60 and 90 fs routinely available from higher-power Cr:ZnS/Cr:ZnSe laser systems [24,25,29]. Alternatively, thulium-doped femtosecond fiber systems can also directly provide 100 fs pulses with no extra nonlinear spectral broadening stages at over 100 W of average power [30]. Assuming 30, 60, and 90 fs Gaussian driving pulses with a central wavelength of 2.3 μm

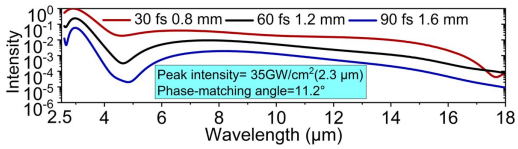

Fig. 5. Simulated output spectra from the cascaded IDFG process in a GaSe crystal driven by longer pulses.

and a fixed peak intensity of 35 GW/cm^2, we simulated the corresponding MIR output by using a GaSe with a thickness of 0.8, 1.2, and 1.6 mm (see Fig. 5). Thicker GaSe crystals are used for longer pulses to compensate for the reduction of MIR conversion efficiency. The simulated spectra also show a very broad coverage from these driving pulses, illustrating the potential of using the more readily available longer pulses from high-power 2 μm sources.

In conclusion, we have experimentally demonstrated, for the first time to the best of our knowledge, the use of cascaded IDFG in the MIR to generate multi-octave spectra using significantly longer pulses than possible with non-cascaded IDFG alone. The demonstration was carried out using a straightforward Cr:ZnS master-oscillator power-amplifier system, providing 3.35 W of average power and 28 fs of pulse duration with no further dedicated nonlinear compression stages. This modest amount of pulse energy, in principle, can also be provided by a single high-power Cr:ZnS oscillator with a lower repetition rate. The resulting broad MIR output after IDFG spans from 2.7 μm to at least 17 μm (590 to 3700 cm^{-1}). Together with the co-propagating driving beam, the system simultaneously covers the majority of the 2–20 μm MIR range. According to simulations, similar broad IDFG spectra can also be obtained with even longer (up to 90 fs) driving pulses that are much more widely available. While further experiments are needed to verify the few-cycle and CEP-stabilized nature of the pulses, the findings already open the way to a substantially more accessible and robust scheme for generating coherent broadband MIR radiation. The combination of alignment-insensitive single-beam geometry, ultra-broadband MIR coverage, femtosecond output pulse duration, and intrinsic CEP stabilization of a significant part of the spectrum, all of which driven by a simple mode-locked laser, make the presented cascaded IDFG scheme one of the most promising sources for emerging nano-imaging [31,32], frequency comb [33,34], and time-domain spectroscopy techniques [31].

Funding. China Scholarship Council (CSC) (201706035015); Centre for Advanced Laser Applications (CALA).

Acknowledgment. The authors thank Prof. Ferenc Krausz for valuable discussions. This Letter is supported by CALA. Qing Wang acknowledges the support from CSC.

[†]Authors contributed equally to this work.

REFERENCES

1. P. Hannaford, *Femtosecond Laser Spectroscopy*, 1st ed. (Springer, 2005).
2. J. Haas and B. Mizaikoff, Annu. Rev. Anal. Chem. **9**, 45 (2016).
3. H. Yang, S. Yang, J. Kong, A. Dong, and S. Yu, Nat. Protoc. **10**, 382 (2015).
4. T. Steinle, F. Neubrech, A. Steinmann, X. Yin, and H. Giessen, Opt. Express **23**, 11105 (2015).
5. C. R. Petersen, U. Møller, I. Kubat, B. Zhou, S. Dupont, J. Ramsay, T. Benson, S. Sujecki, N. Abdel-Moneim, Z. Tang, D. Furniss, A. Seddon, and O. Bang, Nat. Photonics **8**, 830 (2014).
6. A. A. Lanin, A. A. Voronin, A. B. Fedotov, and A. M. Zheltikov, Sci. Rep. **4**, 6670 (2014).
7. H. Timmers, A. Kowligy, A. Lind, F. C. Cruz, N. Nader, M. Silfies, G. Ycas, T. K. Allison, P. G. Schunemann, S. B. Papp, and S. A. Diddams, Optica **5**, 727 (2018).
8. H. J. Bakker and J. L. Skinner, Chem. Rev. **110**, 1498 (2010).
9. G. J. Ellis and M. C. Martin, Eur. Polym. J. **81**, 505 (2016).
10. R. Patrick and C. Federico, Laser Photonics Rev. **9**, 452 (2015).
11. S. Xie, N. Tolstik, J. C. Travers, E. Sorokin, C. Caillaud, J. Troles, P. S. J. Russell, and I. T. Sorokina, Opt. Express **24**, 12406 (2016).
12. F. Keilmann and S. Amarie, J. Infrared Millim. Terahertz Waves **33**, 479 (2012).
13. V. O. Smolski, S. Vasilyev, P. G. Schunemann, S. B. Mirov, and K. L. Vodopyanov, Opt. Lett. **40**, 2906 (2015).
14. A. V. Muraviev, V. O. Smolski, Z. E. Loparo, and K. L. Vodopyanov, Nat. Photonics **12**, 209 (2018).
15. R. Huber, A. Brodschelm, F. Tauser, and A. Leitenstorfer, Appl. Phys. Lett. **76**, 3191 (2000).
16. I. Pupeza, D. Sánchez, J. Zhang, N. Lilienfein, M. Seidel, N. Karpowicz, T. Paasch-Colberg, I. Znakovskaya, M. Pescher, W. Schweinberger, V. Pervak, E. Fill, O. Pronin, Z. Wei, F. Krausz, A. Apolonski, and J. Biegert, Nat. Photonics **9**, 721 (2015).
17. J. Zhang, K. Fai Mak, N. Nagl, M. Seidel, D. Bauer, D. Sutter, V. Pervak, F. Krausz, and O. Pronin, Light Sci. Appl. **7**, 17180 (2018).
18. C. Gaida, M. Gebhardt, T. Heuermann, F. Stutzki, C. Jauregui, J. Antonio-Lopez, A. Schülzgen, R. Amezcua-Correa, A. Tünnermann, I. Pupeza, and J. Limpert, Light Sci. Appl. **7**, 94 (2018).
19. O. Novák, P. R. Krogen, T. Kroh, T. Mocek, F. X. Kärtner, and K.-H. Hong, Opt. Lett. **43**, 1335 (2018).
20. Q. Wang, J. Zhang, A. Kessel, N. Nagl, V. Pervak, O. Pronin, and K. F. Mak, in *Laser Congress 2018 (ASSL)*, OSA Technical Digest, Boston, Massachusetts, November 4–8 (OSA, 2018), paper ATu6A.4.
21. S. Vasilyev, I. S. Moskalev, V. O. Smolski, J. M. Peppers, M. Mirov, A. V. Muraviev, K. Zawilski, P. G. Schunemann, S. B. Mirov, K. L. Vodopyanov, and V. P. Gapontsev, Optica **6**, 111 (2019).
22. A. Kessel, S. A. Trushin, N. Karpowicz, C. Skrobol, S. Klingebiel, C. Wandt, and S. Karsch, Opt. Express **24**, 5628 (2016).
23. Y. Yin, X. Ren, A. Chew, J. Li, Y. Wang, F. Zhuang, Y. Wu, and Z. Chang, Sci. Rep. **7**, 11097 (2017).
24. S. B. Mirov, V. V. Fedorov, D. Martyshkin, I. S. Moskalev, M. Mirov, and S. Vasilyev, IEEE J. Sel. Top. Quantum Electron. **21**, 292 (2015).
25. S. Vasilyev, I. Moskalev, M. Mirov, V. Smolski, S. Mirov, and V. Gapontsev, Opt. Mater. Express **7**, 2636 (2017).
26. K. L. Vodopyanov, J. Opt. Soc. Am. B **10**, 1723 (1993).
27. K. Liu, J. Xu, and X. C. Zhang, Appl. Phys. Lett. **85**, 863 (2004).
28. C. Kübler, R. Huber, S. Tübel, and A. Leitenstorfer, Appl. Phys. Lett. **85**, 3360 (2004).
29. I. T. Sorokina and E. Sorokin, IEEE J. Sel. Top. Quantum Electron. **21**, 273 (2015).
30. M. Gebhardt, C. Gaida, F. Stutzki, R. Klas, M. Tschernajew, S. Demmler, C. Jauregui, J. Rothhardt, J. Limpert, and A. Tünnermann, in *Conference on Lasers and Electro-Optics Europe & European Quantum Electronics Conference (CLEO/Europe-EQEC)* Munich, June 25 (2017), paper CJ_11_1.
31. M. Eisele, T. L. Cocker, M. A. Huber, M. Plankl, L. Viti, D. Ercolani, L. Sorba, M. S. Vitiello, and R. Huber, Nat. Photonics **8**, 841 (2014).
32. I. Amenabar, S. Poly, M. Goikoetxea, W. Nuansing, P. Lasch, and R. Hillenbrand, Nat. Commun. **8**, 14402 (2017).
33. A. Schliesser, N. Picqué, and T. W. Hänsch, Nat. Photonics **6**, 440 (2012).
34. I. Coddington, N. Newbury, and W. Swann, Optica **3**, 414 (2016).